Geophysical Research Letters

RESEARCH LETTER
10.1029/2019GL086043

Observed Subdecadal Variations of European Summer Temperatures

W.A. Müller[1], L. Borchert[1,2], and R. Ghosh[1]

[1]Max-Planck Institute for Meteorology, Hamburg, Germany, [2]Sorbonne Universites, LOCEAN Laboratoriy, Institute Pierre Simon Laplace (IPSL), Paris, France

Key Points:
- Observed European summer temperatures exhibit significant subdecadal variations
- The summer temperature variations are connected to the coupled subdecadal North Atlantic climate system
- The subdecadal pathway consists of a barotropic atmosphere, a shift of the jet position, and changes of the blocking frequency

Supporting Information:
- Supporting Information S1
- Figure S1
- Figure S2
- Figure S3
- Figure S4
- Figure S5
- Figure S6

Correspondence to:
W. A. Müller,
wolfgang.mueller@mpimet.mpg.de

Citation:
Müller, W. A., Borchert, L., & Ghosh, R. (2020). Observed subdecadal variations of European summer temperatures. *Geophysical Research Letters*, *47*, e2019GL086043. https://doi.org/10.1029/2019GL086043

Received 4 NOV 2019
Accepted 22 DEC 2019
Accepted article online 26 DEC 2019

Abstract We identify subdecadal variations in European summer temperatures in coupled and uncoupled century-long reanalyses. Spectral analyses reveal significant peaks at 5–10 years in the midtwentieth century. The subdecadal variations show substantial amplitudes of ~1–1.5 °C, associated with extremely warm summers during their positive phases. We use forced ocean model experiments and show that the European summer temperature variations are associated with the subdecadal coupled North Atlantic climate system. A positive winter NAO-like forcing is associated with changes in the ocean circulation and mass and heat convergence occurring 1–2 years prior to European summer temperature rise. Ocean heat content and sea surface temperature increase in the subtropical North Atlantic. The atmospheric response is barotropic and induces wave activity fluxes toward the European continent, modulation of the jet positions, and blocking frequency. The atmospheric response establishes a pathway connecting the subdecadal coupled North Atlantic climate system to European summer temperature.

1. Introduction

The observed European summer temperatures have increased by ~1.5–2 °C since the 1990s and are expected to increase further due to the global mean temperature rise associated with increasing greenhouse gas (GHG) emissions (Christidis et al., 2015; Schär et al., 2004; Suárez-Gutiérrez et al., 2018). The internal variability of European summer temperatures, however, exhibits magnitudes of similar value (~1.5–2 °C) as the observed temperature rise and can therefore not be neglected for the attribution of extreme events and the distinguishability of their likelihood of occurrence within the limit targets set by UNFCCC Paris Agreement (Suárez-Gutiérrez et al., 2018). Source of the internal variability, however, shows a rich diversity ranging from a random appearance, local coupled soil-atmosphere feedbacks (Seneviratne et al., 2006) to multidecadal variations forced by the inertia of the Atlantic Ocean (Gastineau & Frankignoul, 2015; Ghosh et al., 2016). For example, Figure 1 shows the development of central European summer temperatures and indicates prominent variations of year-to-year, multidecadal time scales and the recent trend. Moreover, summer temperatures show appearances of a subdecadal persistence of relatively warm and cold summers, a persistence that has not yet been examined. In this study, we use the century-long reanalyses of the NOAA 20th century (Compo et al., 2011) and the ECMWF ERA-20C (Poli et al., 2016) and CERA-20C (Laloyaux et al., 2018), in addition to forced ocean model experiments with the Max-Planck-Institute Ocean model (MPIOM), and identify new subdecadal variations of European summer temperature linked to the internal variations of the coupled North Atlantic climate system.

Subdecadal climate variations (SDV) have a significant signature in the internal variability of the coupled North Atlantic climate system. Spectral peaks at ~5–10 years have been found for a number of ocean-related quantities including observed sea surface temperatures and Gulf Steam indices (Czaja & Marshall, 2001; McCarthy et al., 2018) or heat content and overturning stream functions (Martin et al., 2019). Prominent winter sea-level pressure (SLP) patterns such as the subtropical high or the Icelandic low reveal peaks at subdecadal time scales (Czaja & Marshall, 2001). A significant spectral peak at ~9 years has also been found for the North Atlantic Oscillation (NAO; Da Costa & Verdiere, 2002). Observations and modeling results indicate an active role of the atmospheric heat and momentum forcing from the winter NAO, together with a delayed effect of the redistribution of North Atlantic water masses on a subdecadal to decadal time scale (Czaja & Marshall, 2001; Eden & Greatbatch, 2003; Martin et al., 2019; Reintges et al., 2017). Others noted the relative importance of the Arctic sea ice (Deser & Blackmon, 1993) and remote forcing such as the decadal variations of El Niño/Southern Oscillation (ENSO) with the NAO (Müller et al., 2008).

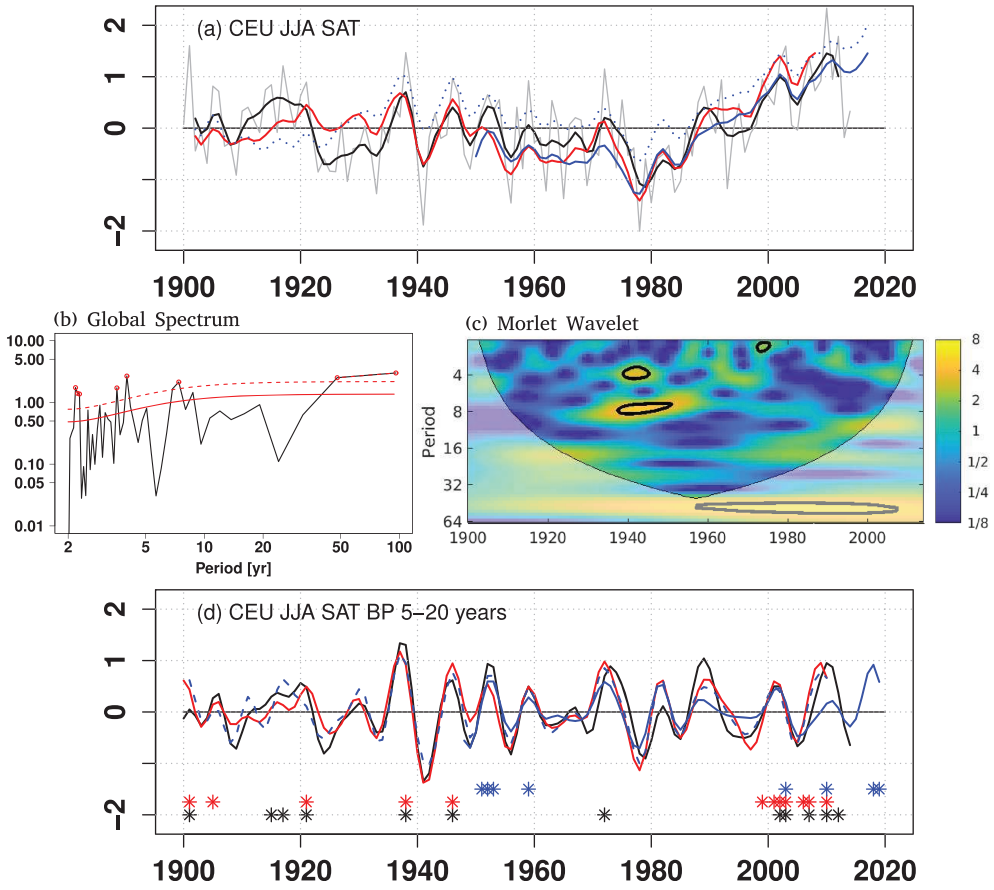

Figure 1. Subdecadal frequency of central European summer air temperature (CEU_SAT). (a) Time series of CEU_SAT averaged over the region 0–40°E, 40–60°N. Shown are summer (JJA) means for NOAA-20CR (gray) and running 5-year mean summer CEU_SAT of NOAA-20CR (black), ERA-20C (red), CAMS (blue), and HadCRUT Version 4 (blue dotted) for the period 1900–2019. (b) Global amplitude spectrum of summer CEU_SAT (black) and AR(1) process (red) for NOAA 20CR. Dashed red line shows the Chi-squared 95% interval. Dotted shown the significant values of CEU_SAT (c) Morlet wavelet spectrum of summer CEU_SAT for NOAA-20CR. Black lines indicate the 95% significance level with respect to an AR(1) process, and shaded areas indicate the cone of influence. (d) The 5- to 20-year band-pass filtered summer CEU_SAT for NOAA-20CR (black), ERA-20C (red), CERA-20C (blue dashed), and CAMS (blue solid). Stars denote linear detrended summer means exceeding the upper 90th percentile of NOAA-20CR (black), ERA-20C (red), and CAMS (blue).

While the subdecadal variations of the North Atlantic climate system are well established, their impacts on continental scale have received less attention. A link from the SDV of the winter NAO onto the northern European winter climate has been assessed (Årthun et al., 2017; Reintges et al., 2017). Årthun et al. (2017) found that variations in the ocean temperature in the high-latitude North Atlantic and the Nordic Seas are reflected in the climate of northwestern Europe and winter Arctic sea ice extent (cf. their Figure 2). However, an analysis to assess the impact on boreal summer has not been performed. In this paper, three questions are addressed: (I) Do European summer temperatures show significant variations on a subdecadal time scale, (II) are the variations of European summer temperatures coupled with the subdecadal North Atlantic climate system, and (III) how would an associated atmospheric pathway look like linking the North Atlantic with European summer temperatures.

2. Data and Methods

2.1. Century-Long Reanalyses and Forced Ocean Model Experiments

To examine the SDV of European summer temperatures and associated atmospheric pathways, we consider data from the NOAA 20th century reanalysis (hereafter NOAA-20CR; Compo et al., 2011) and the ECMWF reanalysis ERA-20C (Poli et al., 2016) and CERA-20C (Laloyaux et al., 2018) from 1900 onward. For

NOAA-20CR, we use an updated version (NOAA-20CRv2c) covering the period 1851–2014. This version corrects for sea ice using COBE-SST2 and enables more observations from the International Surface Pressure Databank Version 3.2.9, compared to the original version. ERA-20C covers the period 1900–2010, and its assimilation includes observations of surface pressure and surface marine winds only. CERA-20C is a 10-member ensemble of coupled climate reanalyses covering the period 1901–2010. It is based on the CERA assimilation system, which assimilates only surface pressure and marine wind observations as well as ocean temperature and salinity profiles (Laloyaux et al., 2018). In this study, we use one member of CERA-20C. In addition, we use the combined land and marine temperature anomalies of the HadCRUT Version 4.6 (Morice et al., 2012) and GHCN_CAMS (Fan & van den Dool, 2008). We consider European summer temperatures for every grid point and with an index defined as the average over the region 0–40° E and 40–60°N (hereafter CEU_SAT).

To examine the SDV in the North Atlantic and its potential source for the SDV of European summer temperatures, two experiments of the MPIOM (Jungclaus et al., 2006) forced with the NOAA-20CR (hereafter NOAAf) and the ERA-20C (ERAf) are used. In both experiments, MPIOM is forced by a number of variables to obtain freshwater and surface fluxes of heat and momentum at the air-sea boundary. The fluxes are estimated with Bulk formulas, and the procedure is described in Müller et al. (2015). For NOAAf, a low-resolving version of MPIOM with a nominal resolution of 1.5° (GR1.5) is used (Jungclaus et al., 2006). NOAAf has been used to examine the historical warming of the North Atlantic during the 1920s (Müller et al., 2015) and decadal to multidecadal variations of ocean mass and heat transport and convergence of the ocean heat content (Borchert et al., 2018; Menary et al., 2013). Based on these ocean estimates, initialized decadal climate predictions of the North Atlantic and hemispheric surface temperatures have been assessed covering the entire twentieth century (Müller et al., 2014, Wu et al., 2019, Borchert et al., 2018; Borchert et al., 2019). For ERAf, experiments have been performed using MPIOM in a higher-resolution setup on a tripolar (TP) grid at nominal 0.4° horizontal resolution (TP04; Jungclaus et al., 2013). For both GR1.5 and TP04, 40 unevenly spaced vertical levels are used with the first 20 levels distributed over the top 700 m. For ERAf, five cycles of the forced experiments have been performed to achieve a stable ocean state. ERAf has demonstrated interannual and multidecadal surface heat fluxes comparable with the reanalyses (cf. figure 7 in Hegerl et al., 2019).

2.2. Analysis Methods

Our analysis is based on correlation and composite methods. The correlation coefficients are calculated with the Pearson formula. Composites are estimated based on the differences between warm and cold phases of the CEU_SAT, which is above or below half a standard deviation. The significances of the correlations and composites are assessed with a resampling method based on a Monte Carlo procedure, where the expected values are calculated by resampling the time series 1,000 times with replacement and determination of the 95% confidence intervals. Values are considered significant when lying outside the confidence intervals. To account for the autocorrelation, a resampling of blocks with 10-year length is used (Wilks, 1997).

A wavelet technique is used to estimate the local power spectrum of the CEU_SAT (Grinsted et al., 2004). To account for the boundary effects, a cone of influence is defined as the area in which the power has dropped to e^{-2} of the value at the edge. The statistical significance is assessed with the null hypothesis that a first-order autoregressive process is giving the background power spectrum. Once the time-frequency space is established, the time series can be filtered by an inverse transformation. Here we filter in a 5- to 20-year frequency band.

For the examination of the dynamical response of the atmosphere to SST, we use dynamical diagnostics such as the maximum Eady (1949) growth rate (EGR) as a measure of the baroclinic instability and the wave activity flux (WAF) to assess the vertical and horizontal propagation of momentum of Rossby wave packages (Takaya & Nakamura, 2001). Both measures are further defined in the supporting information.

Further, the atmospheric blocking is calculated using the two-dimensional blocking index by Scherrer et al. (2006). This index considers all latitudes between 35°N and 75°N as central latitudes, and a daily 500-hPa geopotential height (z500) gradient is determined with respect to the latitude gradient of 15° north and south of every central latitude. A grid point is considered as blocked when the northern and southern z500 gradients are less than −10 m and more than 0 m, respectively, for at least 5 consecutive days.

All time series are calculated by first defining the anomalies with respect to the climatology and then seasonally averaging of the anomalies. For NOAA-20CR, ERA-20C, and CERA-20C, we consider the full period. For HadCRUT4, the anomalies are defined with respect to 1961–1990 climatology (Morice et al., 2012). We examine winter and summer seasons as January-February-March and June-July-August averages. In section 3, extreme temperatures are considered. Here an extreme is defined as the summer temperature exceeding the 90th percentile of the averaged detrended time series. In sections 4 and 5, we focus on the 5- to 20-year band-pass filtered data, and the analysis is performed for the period 1920–1960.

3. Subdecadal Variations of European Summer Temperatures

First, the spectral analyses are used to detect significant frequencies of the CEU_SAT. The global power spectrum reveals significant amplitudes at subdecadal frequencies of ~8–10 years, in addition to significant peaks at interannual and multidecadal time scales (Figure 1b). The subdecadal frequency is in line with other studies showing significant peaks for oceanic and atmospheric quantities of the North Atlantic climate system (see section 1). A local wavelet-analysis reveals that a significant period of the subdecadal frequency appears during the 1920s to the 1960s and higher amplitudes from the 2000s onward (Figure 1c). The amplitudes of the subdecadal variations of CEU_SAT are relatively prominent with magnitudes of ~1–1.5 °C, as can also be inferred from the wavelet 5- to 20-year band-pass filtered time series (Figure 1d). The band-pass filtered time series underline an active subdecadal period during 1920–1960 and prominent variation during the 2000s. It is worth noting that a similar wavelet spectral analysis with other reanalysis (e.g., ERA-20C and CERA-20C) and HadCRUT also reveal significant amplitudes within the 5- to 20 year frequency band but within a smaller time window during this period.

The band-pass filtered time series further reveal a close relationship to extremely warm summers (Figure 1d). For CAMS, all extremes coincide with the positive phase of SDV. For NOAA-20CR (ERA-20C), 11 out of 12 (10/12) extremely warm summers occur when SDV is in a positive phase. Noteworthy, all extremes during the 2000s are associated with positive SDV. A period with reduced likelihood of occurrence of extremes is shown from late 1970s to 1990s, which is associated with a negative phase of the multidecadal variations (e.g., Borchert et al., 2019).

To assess the origin of the subdecadal variation of CEU_SAT, a correlation analysis is performed with NOAA-20CR global surface temperatures (Figure 2). For the period 1920–1960, significant correlation of $r \geq 0.8$ shows up with sea surface temperatures in the subtropical North Atlantic. Elsewhere, the correlations are unstructured, though locally significant values occur. A similar correlation analysis but for the period 1960–2000 reveals that CEU_SAT is directly related to the tropical and extratropical Pacific. This shows the nonstationary character of the subdecadal variations and suggest that other climate processes outside the North Atlantic climate system influence the SDV of European summer temperatures. For example, previous work has examined the complex phase relationships of the climate modes (ENSO and NAO) on decadal time scales (Müller et al., 2008). They find an in-phase relationship between the decadal ENSO and the NAO before the 1960s suggesting a potential driver for SDV of the North Atlantic climate system. Afterward, the decadal ENSO tends to precede the NAO. However, an analysis about the phase relationships of these climate modes is beyond the scope of this analysis, and well-designed experiments could disentangle the question of forcing and nonstationarity of CEU_SAT SDV more adequately. Since the wavelet spectral analysis shows significance during the midtwentieth century, in the following, we focus on the impact of the North Atlantic on CEU_SAT within the period 1920–1960.

4. A Subdecadal Coupled North Atlantic Climate System

A lead-lag correlation of CEU_SAT with SLP is used to examine the processes leading to the significant correlations of CEU_SAT with the North Atlantic SST. During summer and lead 0 year, the CEU_SAT are positively correlated with SLP anomalies over the subtropical North Atlantic and negatively correlated with SLP over higher latitudes (Figure 3, here shown NOAA-20CR). With increasing lead of SLP, the correlations become weaker, and at lead 3–4 years, a phase reversal appears. A similar analysis with the winter SLP reveals a weaker correlation with CEU_SAT at lead 0 years compared to the summer SLP, but for larger lead times (1–2 years), a strong NAO-like SLP structure becomes apparent. A similar analysis with ERA-20C

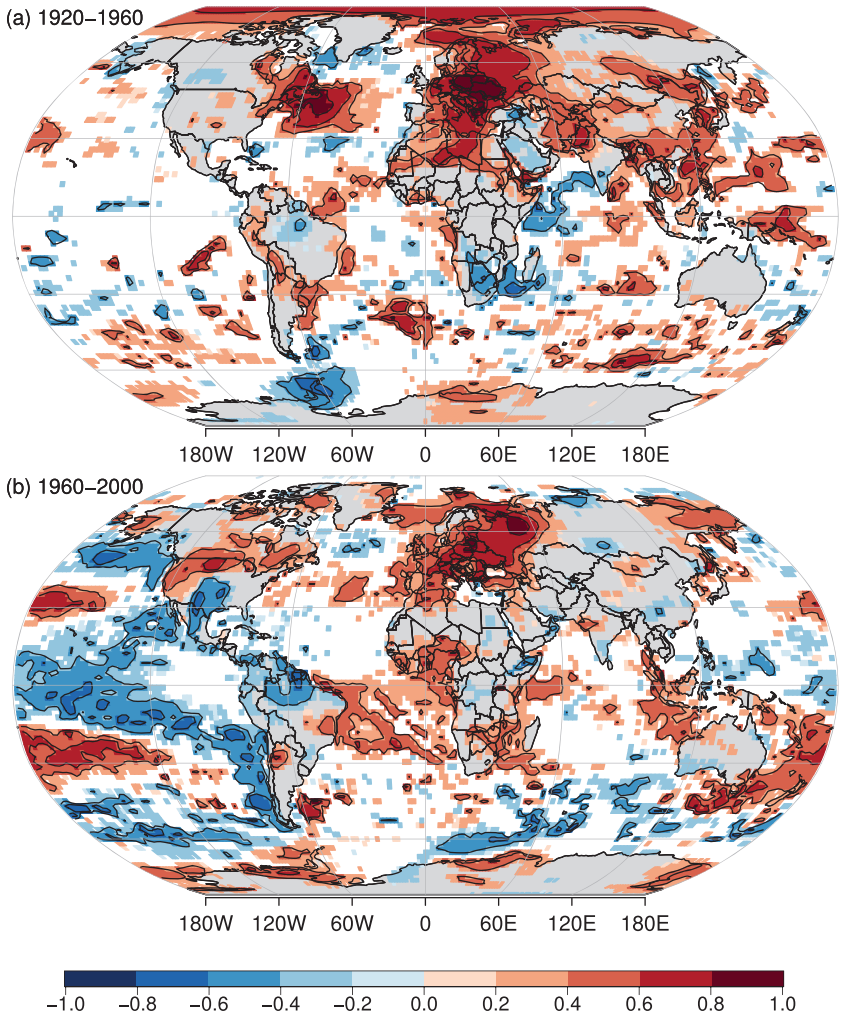

Figure 2. Global correlations of subdecadal European summer temperatures. Anomaly correlations of CEU_SAT with summer surface temperature for the period (a) 1920–1960 and (b) 1960–2000. Colors indicate significant values exceeding the 95% confidence levels based on a resampling method. Here we used the 5- to 20-year band-pass filtered data of the NOAA-20CR.

(Figure S5) and CERA-20C (not shown) reveals the same distribution of SLP, though the winter NAO is more prominent in ERA-20C compared to NOAA-20C. A lead-lag correlation of CEU_SAT with the winter North Atlantic SLP difference and the Hurrell winter NAO index confirms that a NAO-like winter SLP pattern precedes the summer CEU_SAT by ~1–2 years (Figure 4a).

Previous studies have shown that winter NAO-like circulation patterns and associated surface heat and momentum forcing precede North Atlantic Ocean circulation and heat content adjustments as part of a subdecadal coupled system (Martin et al., 2019; Reintges et al., 2017). Further, positive heat content anomalies in the subtropical Atlantic can emerge 2–3 years after a strong NAO. The question is could the summer subtropical SST, SLP, and thus CEU_SAT be part of such subdecadal coupling in the North Atlantic? To investigate this, we use the ocean model experiments forced with the century-long reanalyses (NOAAf and ERAf). In the following, results are shown from the perspective of CEU_SAT, and "minus years" indicates SAT summer temperatures lag the considered variable.

For ERAf, the correlations of CEU_SAT with winter surface downward heat fluxes reveal heat fluxes into the atmosphere in the subpolar region at minus 1–2 years, when a positive NAO-like SLP is most pronounced (Figures 4b and S1). Similarly, heat fluxes into the subtropical North Atlantic are found at minus 1–2 years. From lead 0 onward, the surface heat flux anomalies are reduced and reversed in both regions. In association

Figure 3. Correlation of subdecadal CEU_SAT with sea-level pressure for the midtwentieth century (1920–1960). Shown are the correlation coefficients for (a–e) summer and (f–j) winter sea-level pressure leading the CEU_SAT by (a, f) 4 years, (b, g) 3 years, (c, h) 2 years, (d, i) 1 year, and (e, j) 0 years. Here we used the 5- to 20-year band-pass filtered data from the NOAA-20CR.

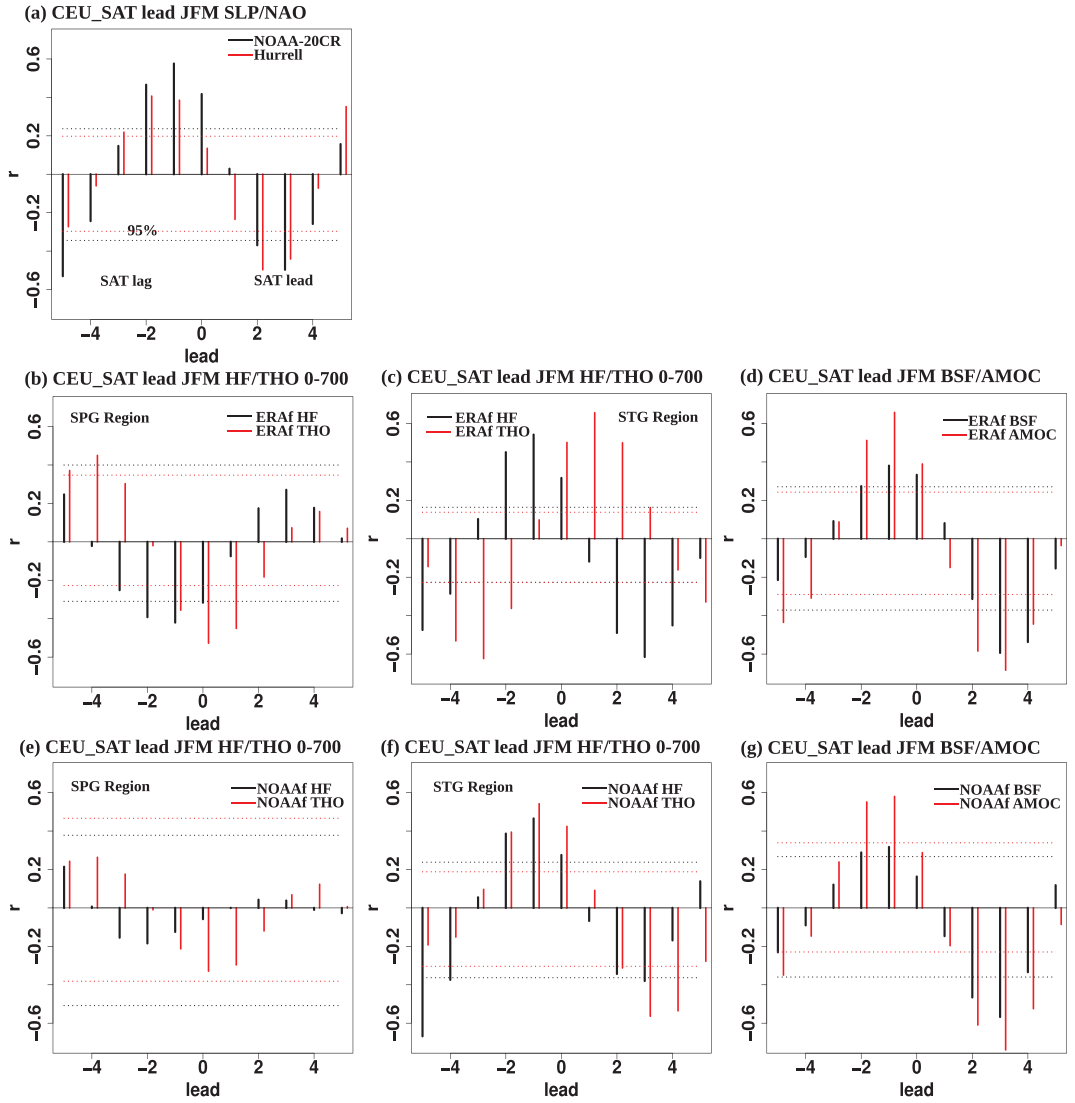

Figure 4. Relation of CEU_SAT with subdecadal coupled North Atlantic system in forced ocean experiments for the mid-twentieth century (1920–1960). Lead-lag correlations of the CEU_SAT with (a) SLP difference (black, 80°W to 0°, 30–50°N minus 60°W to 20°E,60–80°N; see boxes in Figure 3h for averages) and the Hurrell NAO index (red, Hurrell (1995)) for winter. Also shown the correlations of (b) surface downward heat flux (black, 60–20°W, 50–65°N) and ocean temperature 0–700 m (red, 60–20°W, 50–65°N) in the subpolar gyre region, (c) the surface downward heat flux (black, 80–50°W, 30–50°N), and ocean temperature 0–700 m (red, 80–50°W, 30–50°N) in the subtropical gyre region, and (d) the barotropic stream function (red, 80–20°W, 40–50°N) and dipolar AMOC (black, 25–40°N minus 45–60°N). The AMOC is averaged for 0–2,000 m. See boxes in Figures S1 and S2 for the averages. The variables are taken from the ERAf experiment. (e–g) Similar to (b)–(d) but for the NOAAf experiment. The horizontal lines indicate the 95% confidence levels based on 1,000 times resampling. Here we used the 5- to 20-year band-pass filtered data.

indicating a northward shift and strengthening of the Gulf stream (Figures 4d and S2; McCarthy et al., 2018). The Atlantic meridional overturning circulation (AMOC) exhibits a dipolar structure with a maximum at 25–40°N and a minimum at 45–60°N, implying mass transport and heat convergence at ~40°N (Figure S2). The highest amplitude of the dipolar structure of the AMOC is found at minus 1–2 years, similar to the barotropic stream function. Both barotropic stream function anomalies and the dipolar structure of the AMOC are subsequently reduced and the phases reversed 4 years later. A similar dynamical response is shown in NOAAf (Figure 4g).

The forced experiments show that the increase of ocean heat content in the STG region and respective SST during summer, such as shown in the reanalyses (Figures 2a and S4), is an effect of the

subdecadal coupling process resulting from a NAO-like ocean forcing preceding 1–2 years. Surface heat fluxes and the modulation of gyre strength and AMOC explain the increase of heat content and SST.

Though the forced experiments and reanalyses provide similar SST anomalies with respect to the CEU_SAT, it is unclear how the ocean can feed back to the atmosphere and lead to the subdecadal CEU_SAT variations. Correlations of total summer heat flux with CEU_SAT at lead 0 give some indications (Figure S3). The positive correlations in the region 30–55°N in ERAf, NOAA-20CR, and CERA-20C reveal heat flux into the ocean and thus support the increase of SST in this region (Figures 2a and S4). As such the SST does not act as the driving agent for the subdecadal variations of CEU_SAT. However, ERAf and CERA-20C also show negative correlation in the Caribbean region and indicate heat flux into the atmosphere. This region has been identified as an important driver of variations during the twentieth century of the summertime climate of both North America and western Europe (Hodson et al., 2010) and seems also be relevant to the subdecadal time scale.

There are however regional differences of the heat flux distributions among the experiments and reanalysis, inhibiting a clear conclusion concerning the driver of the CEU_SAT at this point. The negative heat flux correlation is only shown in ERAf and CERA-20C but not in NOAA-20CR. This can be related to the AMP-design of NOAA-20CR, in which the heat flux missing coupled feedbacks from the ocean. Further, the location of the negative heat flux correlation does not fully overlap in ERAf and CERA-20C. Here some well-designed experiments could disentangle the drivers.

5. A Subdecadal Atmospheric Pathway

We next consider the subdecadal atmospheric pathway associated with CEU_SAT. Composites of upper-level atmospheric variables show a significant difference between positive and negative phases of the subdecadal CEU_SAT. The geopotential at 500 hPa (z500) shows positive values over the central Atlantic and Europe and negative values over northern North Atlantic (Figure 5a). The amplitudes of the subdecadal z500 anomalies reach up to 40 hPa. This pattern is similar to the SLP and indicates an equivalent barotropic atmospheric structure. Similar SLP and z500 patterns are found for ERA-20C and CERA-20C (Figure S6) and indicate a robust subdecadal pathway between the reanalyses. However, over the Eurasian continent, the centers of action diverge indicating the regional sensitivity of the surface temperature with respect to the teleconnections in the reanalyses. This can explain the different significance found in the wavelet spectrum for a fixed area such as CEU_SAT. It should also be noted that this atmospheric response is different from the multidecadal SST and heat flux anomalies, for which a weak baroclinic geostrophic adjustment has been found (e.g., Gastineau & Frankignoul, 2015; Ghosh et al., 2016).

Zonal winds at 200 hPa shows anomalies of $\pm$5 m/s over the North Atlantic and reveals a northward shift of the jet location during positive phases of the CEU_SAT and vice versa (Figure 5b). This is associated with a northward shift of the storm tracks (not shown). Over the Eurasian continent, zonal wind anomalies with similar magnitude indicate a southward displacement and a strengthening of the Asian jet during the positive phases of CEU_SAT. Further, atmospheric blocking is favored over central to Eastern Europe during the positive phases of CEU_SAT, with a significant increase of the percentage of blocked days per season, while the blocking frequency is decreased over Northwest Europe (Figure 5c). Thus, during the positive phase of the subdecadal variation of CEU_SAT, such high pressure and associated increase of blocking frequency favor extreme temperatures (see also Figure 1d).

Lastly, we examine the dynamical context of the atmospheric response for the different SDV phases by the EGR and the WAF. The EGR shows a northward shift of the most unstable synoptic disturbances in the North Atlantic for the positive phases of SDV (Figure 5d). This is in agreement with the corresponding displacement of the upper-level jet and storm-track position. The vertical component of the WAF reveals ascending momentum transport of Rossby wave packages over the western North Atlantic, located west of the geopotential high anomaly. The horizontal WAF further indicates a propagation of stationary Rossby waves, generated from the northwest Atlantic, toward the central-to-eastern Europe. A convergence of WAF flux is located at the central North Atlantic, which indicates an eddy-mediated feedback onto the mean flow.

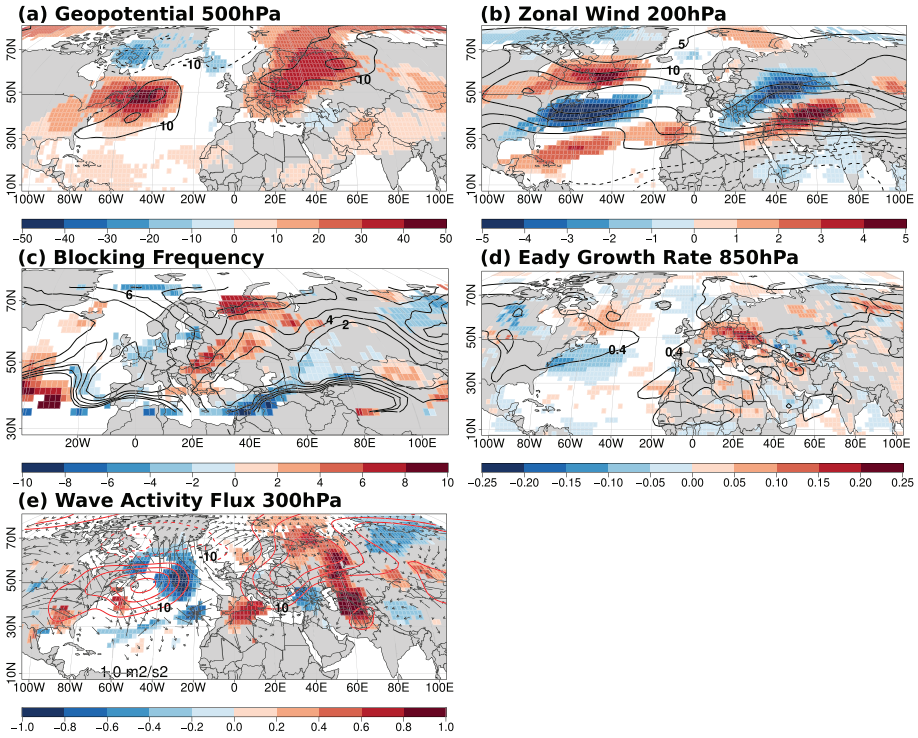

Figure 5. Subdecadal atmospheric pathway from subtropical SST to CEU_SAT during summer for the midtwentieth century (1920–1960). Shown are composites defined with respect to the positive minus negative phases of the 5- to 20-year band-pass filtered CEU_SAT. Positive (negative) phases are defined when the index exceeds 0.5 (−0.5) standard deviation. Shown are composites for (a) geopotential at 500 hPa (shadings, 10 hPa) alongside with SLP (contours, 10 hPa), (b) zonal wind at 200 hPa (shadings, 1 m/s) together with the zonal wind climatology (contours, 5 m/s), (c) blocking frequency (shadings, percentage of blocked days per season) and its climatology (contours, every 2% of blocked days per season), (d) Eady growth rate (shadings, 0.05 day^{-1}) and the Eady growth rate climatology (contours, 0.4 day^{-1}), and (e) the wave activity flux horizontal (vectors, 1 m^2/s^2) and vertical (shadings, 10^{-2} m^2/s^2) components and geopotential at 500 hPa from (a) in contours (10 hPa). Only every second and third vectors are shown in latitude and longitude, respectively The colors indicate significant values with respect to the 95% confidence intervals of a resampling method. Here we used data from the NOAA-20CR.

The atmospheric upper-level diagnostic reveals a subdecadal pathway from the subtropical Atlantic to the European continent. The pathway includes a signature in the baroclinicity via the EGR, but the vertical structure remains mainly equivalent barotropic. This suggests that eddy-feedback processes significantly contribute to the atmospheric adjustment to the diabatic heating (Kushnir et al., 2002). Further, the WAF clearly shows a horizontal structure and indicates that Rossby wave related momentum is transported from the subtropical North Atlantic to the European/Eurasian continent. The WAF also has a weak vertical component over the subtropics. However, it is not clear now whether this is related to the heat release in this region, and further analysis is required.

6. Summary and Conclusion

Using century-long reanalyses, subdecadal variations (SDV) of European summer temperatures are found. The svariations are significant in the midtwentieth century and linked to the subdecadal coupled North Atlantic climate system. NAO-like winter climate modulates the North Atlantic water-mass properties, ocean circulation, and associated mass and heat convergence 1–2 years prior to European summer temperatures. The ocean heat content anomalies are increased in the subtropical North Atlantic. The atmospheric pathway is equivalent barotropic and induces wave activity flux toward the European continent, latitudinal displacement of jet positions, and changes of the blocking frequency. It is the modulation of the atmospheric large-scale circulation that increases the blocking frequency, leading to extremely warm summers during the positive phase of SDV.

The equivalent barotropic structure is different to the weak-baroclinic atmospheric response to multidecadal diabatic heating in the North Atlantic (Ghosh et al., 2016). While for the multidecadal atmospheric response, the effect of eddy-related feedback has been shown to be negligible; the equivalent barotropic structure suggests that eddy momentum fluxes can play a role modulating the surface heating anomaly on subdecadal time scale.

The subdecadal variations exhibit a nonstationary character with significant values during the midtwentieth century and nonsignificant values afterward. This suggests that other climate processes influence the SDV of European summer temperatures. During 1960–2000, the summer temperatures are instantaneously correlated with the Pacific, rather than with the North Atlantic as during 1920–1960. An in-phase relationship however is found between the decadal ENSO and the NAO before the 1960s suggesting a potential driver for SDV of the North Atlantic climate system (Müller et al., 2008). Afterward, the decadal ENSO tends to precede the NAO. An analysis about the complex phase relationships of the climate modes on decadal time scales is beyond the scope of this analysis and well-designed experiments could disentangle the question of forcing and nonstationarity of CEU_SAT SDV more adequately.

The subdecadal variations are shown to be a fundamental component of the internal variability of European summer temperatures and are closely associated with extreme summer temperatures (Figure 1d). It has also been demonstrated that the internal variability of European temperature variations and respective extremes is in the range of the observed mean temperature rise associated with increasing GHG emissions (Suárez-Gutiérrez et al., 2018). As such, we postulate that the additional contributions of the subdecadal and multidecadal processes alongside with the increasing trend due to rising GHG conditions require consideration when attributing extreme heat waves such as those in the 2000s and 2010s.

Acknowledgments
The research leading to these results has received funding from the German Federal Ministry for Education and Research (BMBF) projects MiKlip (Grant 01LP1519A, W. A. M. and L. B.) and ClimXtreme (Grant 01LP1901F, W. A. M.), European H2020 projects AtlantOS and Blue-Action (RG), and European Climate Prediction (EUCP, Grant Agreement 776613, L. B.). The climate simulations were performed at the German Climate Computing Centre (DKRZ). Primary data, scripts, and other supporting information that may be useful in reproducing the author's work are archived by the Max Planck Institute for Meteorology and can be obtained through the institutional repository (http://hdl.handle.net/21.11116/0000-0004-F5E2-8). The authors thank Chao Li, whose comments helped to improve a former version of this paper, and the two reviewers, whose comments substantially improved the submitted version.

References

Årthun, M., Eldevik, T., Viste, E., Drange, H., Furevik, T., Johnson, H. L., & Keenlyside, N. S. (2017). Skillful prediction of northern climate provided by the ocean. *Nature Communications*. https://doi.org/10.1038/ncomms15875

Borchert, L., Düsterhus, A., Brune, S., Müller, W. A., & Beahr, J. (2019). Forecast-oriented assessment of decadal hindcast skill for North Atlantic SST. *Geophysical Research Letters*, *46*, 11. https://doi.org/10.1029/2019GL084758

Borchert, L., Müller, W. A., & Baehr, J. (2018). Atlantic ocean heat transport influences interannual-to-decadal surface temperature predictability in the North Atlantic Region. *Journal of Climate*, *31*, 6763–6782. https://doi.org/10.1175/JCLI-D-17-0734.1

Borchert, L., Pohlmann, H., Baehr, J., Neddermann, N.-C., Suarez-Gutierrez, L., & Müller, W. A. (2019). Decadal predictions of the probability of occurrence for warm summer temperature extremes. *Geophysical Research Letters*. https://doi.org/10.1029/2019GL085385

Christidis, N., Jones, G. S., & Stott, P. A. (2015). Dramatically increasing chance of extremely hot summers since the 2003 European heatwave. Nat. Clim. *Change*, *5*, 46–50.

Compo, G. P., Whitaker, J. S., Sardeshmukh, P. D., Matsui, N., Allan, R. J., Yin, X., et al. (2011). The Twentieth Century Reanalysis Project. *Quarterly Journal of the Royal Meteorological Society*, *137*, 1–28. https://doi.org/10.1002/qj.776

Czaja, A., & Marshall, J. (2001). Observations of atmosphere ocean coupling in the North Atlantic. *Quarterly Journal of the Royal Meteorological Society*, *127*(576), 1893–1916. https://doi.org/10.1002/qj.49712757603

Da Costa, E., & Verdiere, A. (2002). The 7.7 year North Atlantic Oscillation. *Quarterly Journal of the Royal Meteorological Society*, *128*(581), 797–817.

Deser, C., & Blackmon, M. L. (1993). Surface climate variations over the North Atlantic Ocean during winter. *Journal of Climate*, *6*(9), 1743–1753.

Eady, E. T. (1949). Long waves and cyclone waves. *Tellus*, *1*, 33–52.

Eden, C., & Greatbatch, R. J. (2003). A damped decadal oscillation in the North Atlantic climate system. *Journal of Climate*, *16*(24), 4043–4060.

Fan, Y., & van den Dool, H. (2008). A global monthly land surface air temperature analysis for 1948-present. *Journal of Geophysical Research*, *113*, D01103. https://doi.org/10.1029/2007JD008470

Gastineau, G., & Frankignoul, C. (2015). Influence of the North Atlantic SST variability on the atmospheric circulation during the twentieth century. *Journal of Climate*, *28*, 1396–1416. https://doi.org/10.1175/JCLI-D-14-00424.1

Ghosh, R., Müller, W. A., Bader, J., & Baehr, J. (2016). Impact of observed North Atlantic multidecadal variations to European summer climate: A linear baroclinic response to surface heating. *Climate Dynamics*. https://doi.org/10.10007/s00382-016-3283-4

Grinsted, A., Moore, J. C., & Jevrejeva, S. (2004). Application of the cross wavelet transform and wavelet coherence to geophysical time series. *Nonlinear Processes in Geophysics*, *11*, 561566.

Hegerl, G. C. Brönnimann, S., Cowan, T., Friedman, A.R., Hawkins, E., Iles, C. et al. (2019). Causes of climate change over the entire industrial era. ERL-107283

Hodson, D. L., Sutton, R. T., Cassou, C., Keenlyside, N., Okumura, Y., & Zhou, T. (2010). Climate impacts of recent multidecadal changes in Atlantic Ocean sea surface temperature: A multimodel comparison. *Journal of Climate*, *34*, 1041–1058. https://doi.org/10.1007/s00382-009-0571-2

Hurrell, J. W. (1995). Decadal trends in the North Atlantic Oscillation—Regional temperatures and precipitation. *Science*, *269*(5224), 676–679. https://doi.org/10.1126/science.269.5224.676

Jungclaus, J. H., Fischer, N., Haak, H., Lohmann, K., Marotzke, J., Matei, D., et al. (2013). Characteristics of the ocean simulations in MPIOM, the ocean component of the MPI-Earth System Model. *Journal of Advances in Modeling Earth Systems*, *5*, 422–446. https://doi.org/10.1002/jame.20023

Jungclaus, J. H., Keenlyside, N., Botzet, M., Haak, H., Luo, J. J., Latif, M., et al. (2006). Ocean circulation and tropical variability in the coupled model ECHAM5/MPI-OM. *Journal of Climate*, *19*, 3952–3972.

Kushnir, Y., Robinson, W. A., Blade, I., Hall, N. M. J., Peng, S., & Sutton, R. (2002). Atmospheric GCM response to extratropical SST anomalies: Synthesis and evaluation. *Journal of Climate*, *15*, 2233–2256.

Laloyaux, P., de Boisseson, E., Balmaseda, M., Bidlot, J. R., Broennimann, S., Buizza, R., et al. (2018). CERA-20C: A coupled reanalysis of the twentieth century. *Journal of Advances in Modeling Earth Systems*, *10*, 1172–1195. https://doi.org/10.1029/2018MS001273

Martin, T., Reintges, A., & Latif, M. (2019). Coupled North Atlantic sub-decadal variability in CMIP5 models. *Journal of Geophysical Research: Oceans*, *124*, 2404–2417. https://doi.org/10.1029/2018JC014539

McCarthy, G. D., Joyce, T. M. M., & Josey, S. A. (2018). Gulf Stream variability in the context of quasi-decadal and multidecadal Atlantic climate variability. *Geophysical Research Letters*, *45*, 11,257–11,264. https://doi.org/10.1029/2018GL079336

Menary, M. B., Roberts, C. D., Palmer, M. D., Halloran, P. R., Jackson, L., Wood, R. A., et al. (2013). Mechanisms of aerosol-forced AMOC variability in a state of the art climate model. *Journal of Geophysical Research: Oceans*, *118*, 2087–2096. https://doi.org/10.1002/jgrc.20178

Morice, C. P., Kennedy, J. J., Rayner, N. A., & Jones, P. D. (2012). Quantifying uncertainties in global and regional temperature change using an ensemble of observational estimates: The HadCRUT4 data set. *Journal of Geophysical Research*, *117*, D08101. https://doi.org/10.1029/2011JD017187

Müller, W. A., Frankignoul, C., & Chouaib, N. (2008). Observed decadal tropical Pacific-North Atlantic teleconnections. *Geophysical Research Letters*, *35*, L24810. https://doi.org/10.1029/2008GL035901

Müller, W. A., Matei, D., Bersch, M., Jungclaus, J. H., Haak, H., Lohmann, K., et al. (2015). A 20th-century reanalysis forced ocean model to reconstruct North Atlantic climate variation during the 1920s. *Climate Dynamics*. https://doi.org/10.1007/s00382-014-2267-5

Müller, W. A., Pohlmann, H., Sienz, F., & Smith, D. (2014). Decadal climate prediction for the period 1901–2010 with a coupled climate model. *Geophysical Research Letters*, *41*, 2100–2107.

Poli, P., Hersbach, H., Dee, D. P., Berrisford, P., Simmons, A. J., Vitart, F., et al. (2016). ERA-20C: An atmospheric reanalysis of the twentieth century. *Journal of Climate*, *29*, 4083–4097. https://doi.org/10.1175/JCLI-D-15-0556.1

Reintges, A., Latif, M., & Park, W. (2017). Sub-decadal North Atlantic Oscillation variability in observations and the Kiel Climate Model. *Climate Dynamics*, *48*, 3475–3487.

Schär, C., Vidale, P. L., Lüthi, D., Frei, C., Häberli, C., Liniger, M. A., & Appenzeller, C. (2004). The role of increasing temperature variability in European summer heatwaves. *Nature*, *427*, 332–336.

Scherrer, S. C., Croci-Maspoli, M., Schwierz, C., & Appenzeller, C. (2006). Two-dimensional indices of atmospheric blocking and their statistical relationship with winter climate patterns in the Euro-Atlantic region. *International Journal of Climatology*, *26*, 233–249. https://doi.org/10.1002/joc.1250

Seneviratne, S. I., Lü thi, D., Litschi, M., & Schär, C. (2006). Land–atmosphere coupling and climate change in Europe. *Nature*, *443*(7108), 205–209. https://doi.org/10.1038/nature05095

Suárez-Gutiérrez, L., Li, C., Müller, W. A., & Marotzke, J. (2018). Internal variability in European summer temperatures at 1.5 °C and 2 °C of global warming. *European Research Letters* ERL-104665

Takaya, K., & Nakamura, H. (2001). A formulation of a phase-independent wave-activity flux for stationary and migratory quasigeostrophic eddies on a zonally varying basic flow. *Journal of the Atmospheric Sciences*, *58*, 608–627.

Wilks, D. S. (1997). Resampling hypothesis test for autocorrelated fields. *Journal of Climate*, *10*, 65–82.

Wu, B., Zhou, T., Li, C., Müller, W. A., & Lin, J. (2019). Improved decadal prediction of Northern-Hemisphere summer land temperature. *Climate Dynamics*. https://doi.org/10.1007/s00382-019-04658-8